IEEE Access
Multidisciplinary | Rapid Review | Open Access Journal

Received October 14, 2021, accepted November 24, 2021, date of publication December 13, 2021,
date of current version December 27, 2021.

Digital Object Identifier 10.1109/ACCESS.2021.3135190

Modeling and Performance Evaluation of ANFIS Controller-Based Bidirectional Power Management Scheme in Plug-In Electric Vehicles Integrated With Electric Grid

MD. ARIFUL ISLAM[1], JAI GOVIND SINGH[2], (Senior Member, IEEE), ISRAT JAHAN[1], M. S. HOSSAIN LIPU[3,4], TASKIN JAMAL[1,5], (Senior Member, IEEE), RAJVIKRAM MADURAI ELAVARASAN[6,7], AND LUCIAN MIHET-POPA[8], (Senior Member, IEEE)

[1]Department of Electrical and Electronic Engineering, Ahsanullah University of Science and Technology, Dhaka 1208, Bangladesh
[2]Department of Energy, Environment, and Climate Change, School of Environment, Resources and Development, Asian Institute of Technology (AIT), Khlong Nueng, Pathum Thani 12120, Thailand
[3]Department of Electrical, Electronic and Systems Engineering, Universiti Kebangsaan Malaysia, Bangi 43600, Selangor, Malaysia
[4]Centre for Automotive Research (CAR), Universiti Kebangsaan Malaysia, Bangi 43600, Selangor, Malaysia
[5]School of Geography, Geology and the Environment, Keele University, Staffordshire ST5 5BG, U.K.
[6]Department of Electrical and Electronics Engineering, Thiagarajar College of Engineering, Madurai 625015, India
[7]Research and Development Division (Power and Energy), Nestlives Pvt. Ltd., Chennai 600091, India
[8]Faculty of Electrical Engineering, Østfold University College, 1757 Halden, Norway

Corresponding authors: Md. Ariful Islam (md.rahil3@gmail.com) and Lucian Mihet-Popa (lucian.mihet@hiof.no)

This work was supported by the Asian Institute of Technology (AIT) under Grant Asian Development Bank-Japan Scholarship Program (ADB-JSP).

ABSTRACT A bi-directional power exchange between the plug-in electric vehicle (PEV) and the AC electrical grid is necessary to perform the Vehicle to Grid (V2G) and Grid to Vehicle (G2V) operations. While performing these operations, different power converters and controllers play an important role as mediators between the PEV and electric grid. Various works have demonstrated the utilization of controllers for PEV's battery power management. However, the existing conventional controllers have technical shortcomings about vulnerability to controller gain, accurate mathematical modelling, poor adaptability, sluggish response to a sudden outburst and lengthy interval execution processing. Therefore, this paper develops an adaptive neuro-fuzzy inference system (ANFIS) control strategy based bidirectional power management scheme to ensure the optimal electrical power flow exchange between the AC electrical grid and battery storage system in PEVs. This paper aims to reduce the stress on the grid power side and utilize the unused power properly. The performance of the ANFIS model is varied using two PEVs based on real-life power consumptions by different loads at home based on five operational modes. Besides, a comparative analysis between the ANFIS controller and the PI controller is carried out to demonstrate the effectiveness of the proposed control scheme. The results illustrate that the proposed ANFIS controller delivers a smoother power injection from the PEV to the AC power grid with the least harmonics as well as achieves a smoother battery profile and less distortion when power is absorbed by PEV battery.

INDEX TERMS ANFIS controller, plug-in electric vehicle, bidirectional power, state of charge, PI controller.

I. INTRODUCTION

The rising demand for global energy has significantly increased the use of fossil fuels, but they have serious negative impacts on the environment and human health [1]. Thus, to reduce the dependency on traditional energy sources as well as fulfil the energy requirement and manage the global temperature rise, there is a high interest to use not only renewable energy resources but also plug-in electric vehicles (PEVs) [2]–[4]. Because most renewable energy

The associate editor coordinating the review of this manuscript and approving it for publication was Cheng Chin.

resources are intermittent, an energy storage device is usually considered during the system development; nevertheless, the expense of energy storage devices is not always justified [5], [6]. In such a situation, existing energy storage devices, such as PEVs, can play a critical role in terms of cost reduction and storage. PEVs are a new form of electrical load that can be used as a medium of transport and as a medium of energy storage [4]. While each PEV is considered a standalone device, its contribution to the power system is insignificant while performing as an energy storage device. Another driving force of increasing the PEV in the transport and regular use sector is the integration of solar PV in the PEV as a driving source of energy. Particle Swarm Optimization (PSO) based controlled strategy for Photovoltaic System in the purpose of autonomy operation of PEV is also getting popular, but due to intermittency of solar sometimes PEV has to perform G2V operation for charging purpose as well [7]. Multiple recharge-based mathematical modelling, including the traction motor concept of PEV, is getting popular to promote the use of PEV [8]. However, its fast growth in quantity is interfering with the power system stability. Thus, researchers are doing their best to utilize the PEVs collectively in an optimal way to the wellbeing of the power system by operating them in different modes of operation [9]. Two modes of operations are available to connect the PEVs with the power grid. The Grid to Vehicle (G2V) mode is utilized to charge the PEV's battery for mobility purposes and to utilize the unused power during the off-peak hour. Again, the Vehicle to Grid (V2G) mode of operation is utilized to inject power back from PEV to the grid utility system when additional power is required during the peak hour, thus making the power system more reliable [10].

Different types of converters work as mediators for any bi-directional power exchange between PEV and AC power grid. These mediators are also bi-directional power flow converter types. For proper management of different mediators, different controllers are employed according to their performances [11]. Power electronic converters ensure the power exchange between the PEV and power grid, monitor the state of charge (SOC) and regulate the charging/discharging of battery that can enhance the battery life span [12]. Some practical studies combined the DC/DC converter and PI controller for better power management between the AC power grid and PEV [13]. Though the controller's contribution to power system stability is indisputable, its improvement is growing over time. The conventional controller such as Static VAR Compensator (SVC) with cascaded Fractional Order Proportional Integral Derivative controller (FOPID) improves the stability of the power system [14]. PI controller is utilized to recharge the hybrid energy storage system (HESS) to store energy [15]. One study showed that the PI controller applied on the V2G and G2V operation flattened the load power curve without considering the starting overshoot and distortion in PEV's battery power characteristics curve [16]. These overshoot and distortion would reduce the battery's overall performance and life span over time. As PI is a traditional controller, its efficiency can be improved by speeding up its working capability while hybridizing it with artificial intelligence (AI) based controller [17]. Though the PI controller is hybridized by combining with neural networks, still reliability of the controller is a concern to be addressed. Another study showed that fuzzy-based PI controllers could better utilize energy resources by two-way power exchange, fast responses with less steady-state error, and enhanced dynamic flexibility [17]. However, the adaptability fuzzy-based PI controller is an issue to be investigated. These days, the application of PI controller with regard to sophisticated power management is losing its popularity due to its technical limitations like sluggish or no reaction to sudden outburst, concurrence to transient overshoot, vulnerability to controller gain, poor adaptability, large time-delayed processing, precise mathematical modeling, etc. [18]. Controllers like fuzzy and neuro-fuzzy have overcome most of the PI controller's shortcomings. Different mathematical models have been developed to design fuzzy [19] and adaptive neuro-fuzzy controllers (ANFIS) [20].

Fuzzy logic and ANFIS based controllers are viable when a precise mathematical calculation is impossible and load changes are not linear [21]. Fuzzy controllers are even more advantageous where easy tuning is needed with human knowledge or without proper human knowledge. The development of fuzzy logic controller (FLC) is straightforward and cost-effective compared to a traditional PI controller. Moreover, FLC is more robust under a broader range of operations [22]. FLC can be a better choice than a traditional PI controller, where a fast response system is required, but high reliability is still an issue [23]. FLC-based direct torque methodology of a double motor-based PEV has been well explained [24]. A combined direction-based genetic algorithm (GA) and fuzzy inference-based mechanism are utilized on a remotely-operated vehicle (ROV) [25]. With all the advantages of FLC, it is possible to incorporate the combined effect of fuzzy set theory along with artificial neural networks (ANN) to develop an ANFIS method. The ANN integrated FLC makes ANFIS a robust and effective technique. At the same time, the adaptive capability of ANFIS is increased by a trial-and-error process where expert knowledge is not mandatory. In a fuzzy system, rules are generated with human knowledge and manually, where ANFIS generates sufficient rules with the reference of input and output data considering the benefits of ANN. Sometimes, it is not possible to consider all criteria as there are several criteria of weights and position in input choice and assessment procedure. However, ANFIS chooses the finest combination between these criteria to get the maximum output with a minimum error during training operation [26].

ANFIS is utilized as a modern controller by researchers because of its enormous advantages, and it has demonstrated its ingenious performance in different sectors over traditional controllers. ANFIS controller outperforms the traditional controller with respect to time efficiency and optimization

of membership functions (MFs) [27]. The use of ANFIS is broader in modern control systems. However, no suitable study shows the advantage of utilizing an ANFIS controller over a traditional controller. ANFIS makes the system easier in terms of parameter choice and MF optimization and is time-efficient as ANFIS utilizes training data rather than human expert knowledge. Literature shows that ANFIS controllers have been employed to control systems with battery-integrated renewable energy resources better. One study showed that effective battery power management is possible with an ANFIS controller in a hybrid standalone system [28]. Some researchers worked on battery power control of photovoltaic generators with the ANFIS controller [29]. Another work is done on electric power swap between PEV and electrical grid by using ANFIS controller in smart grid [30]. To integrate the PEV with the electrical grid, some researchers emphasized a controller based on AI-based ANFIS [31].

This study aims to model an ANFIS controller and demonstrate the advantages of using this controller over the conventional PI controller. In terms of battery characteristics, this study also illustrates the superiority of the ANFIS controller over the conventional controller. To illustrate the advantages of ANFIS controller over the PI controller, the same power exchange scheme is executed by replacing the two PI controllers with two ANFIS (ANFIS1 and ANFIS2) controllers. With the use of a PI controller, starting surge and a continuous distortion were observed in the battery power and current curves. This distortion continues until battery operation continues, like charging and discharging operations. This starting surge and distortion do not hamper the bi-directional power exchange operation but have a potential threat to battery life span and the system stability over a long period.

In this study, one standard home with two PEVs is considered. A bi-directional power exchange technique reduces the stress on the grid power side and utilizes the unused power properly, with the utilization of G2V and V2G operations. Two ANFIS controllers are developed for the robust operation of battery charging and discharging of PEV with a proposed five steps flexible control strategy. The ANFIS controller is chosen to enable the power exchange between the PEV and the AC power grid. A five operational modes flexible control strategy is developed to regulate this power exchange, thus reducing the grid stress. The proposed five steps flexible control strategy ensures the connection time and charging/discharging duration of each PEV while they are available at home. This control logic aims to determine the connection status of the vehicles in the system when they are available at home and find out the preferred vehicle among them. After that, the SOC value of each connected vehicle is determined and then set their charging/discharging duration for better results. To sum up, the whole study aims to do the following:

- To develop a model which will perform V2G and G2V operations (between the AC power grid and PEVs).

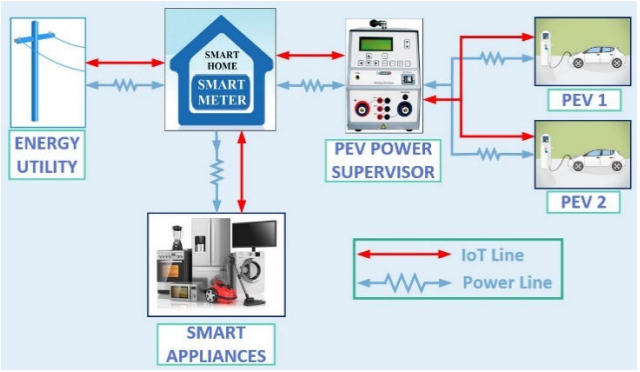

FIGURE 1. Grid-connected smart home with a power converter and smart appliances and PEVs.

- To develop two ANFIS controllers to enable the power exchange between the PEVs and AC power grid.
- To develop a flexible control logic/strategy to perform the V2G and G2V operations efficiently and smoothly.
- Finally, to show the advantages of using ANFIS controller over PI controller.

The study is organized into six sections. The second part describes the considered system and the descriptions of different power converters, sensing circuits, and modelling of PEV's battery. Part 3 shows the details of the proposed five operating modes of the flexible control strategy. Part 4 shows an elaborated description of modelling of two different ANFIS controllers where ANFIS1 is utilized for battery current control and ANFIS2 is utilized for DC bus voltage control. Part 5 shows the simulation and results, and a conclusion is drawn in part 6.

II. SYSTEM MODELLING, WORKING PRINCIPLE, AND EXECUTION PROCESS

A. OVERVIEW OF THE SYSTEM

The paper mainly focuses on modelling different power converters to implement V2G and G2V operation successfully and shows how a modern controller like ANFIS can perform better power management operation than a conventional PI converter. Fig. 1 shows the grid integrated smart home, which includes AC/DC appliances and bi-directional AC/DC power converters.

The battery used in PEV is considered a lithium-ion (Li-ion) battery pack because of its several benefits like long battery life, more usable capacity, constant power, temperature tolerance, and fast-changing safety features [32]. An R-L filter is used on the grid side, ensuring quality power when power is received by the grid or infused from the grid. This R-L filter also helps minimize the harmonics generated by the inverter and ensures a 3-Φ quasi voltage of sinusoidal form. Otherwise, harmonics may distort the grid power quality. A bidirectional AC/DC converter is utilized to exchange power between the AC grid and the DC power link. It works as a rectifier when power flows from the AC grid to the DC power link and as an inverter when power is injected from the DC power link to the AC grid. One

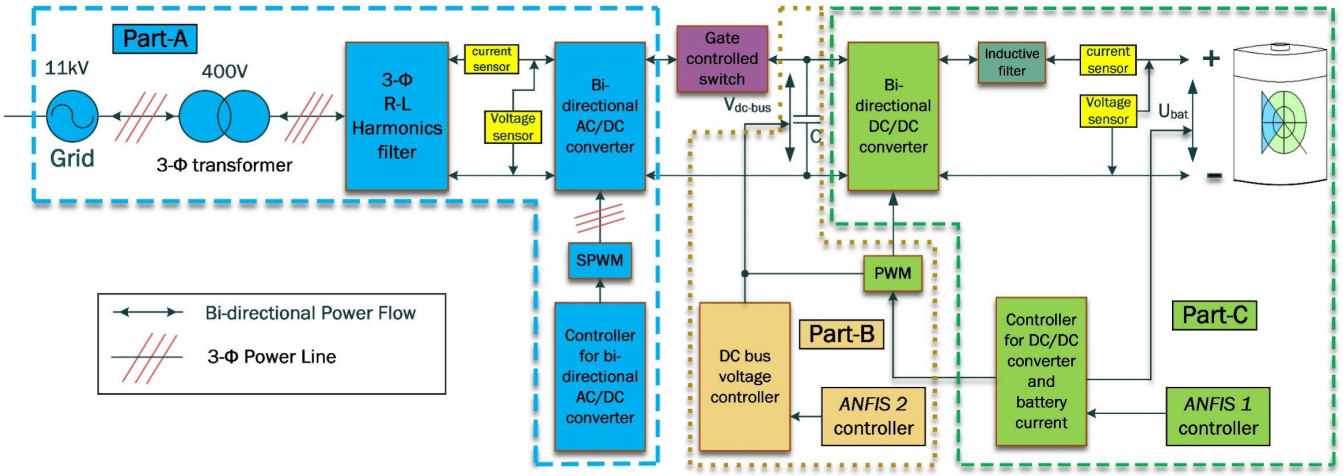

FIGURE 2. Demonstration of different power converters and controllers for power exchange between PEV and grid.

DC/DC switched-mode power supply (SMPS) converter is utilized between the PEV's battery and AC/DC converter. This DC/DC SMPS converter ensures a sufficient voltage level for both the DC bus and battery. The voltage coming from the DC/DC converter ensures a reference DC bus voltage so that the power can be easily injected into the AC grid.

The charging and discharging of the battery are determined by negative and positive battery current, respectively. This charging and discharging battery current may contain ripples that are eliminated by the L filter. Fig. 2 presents an overview of the proposed system, including power converters, controllers, DC link bus voltage, filter, sensing devices, PEV battery, and AC power grid.

B. POWER CONVERTERS AND SENSING DEVICE

Power control between the PEV and electric grid is achieved with the help of different power converters and controllers along with a control algorithm. The converters and their associated controllers are divided into three parts. Part-A shows the bi-directional AC/DC converter along with its associated controller, Part-B shows the DC bus voltage controller, and Part-C shows the DC/DC SMPS and its associated controller.

1) PART-A: BI-DIRECTIONAL AC/DC CONVERTER

To perform the operation of V2G and G2V, there should be bi-directional connectivity between the DC distribution system and AC grid, and in this study, this connectivity is investigated. In Fig. 3, a fully controlled bi-directional 3-Φ AC/DC converter is utilized, and this converter can exchange the power flow at a unity power factor. To connect the AC power grid and the converter, an L filter is utilized. The voltage sources of the AC power grid are denoted as e_a, e_b, e_c and current sources are denoted as i_a, i_b, i_c. The inductance filter is denoted as L, and the resistance of the series $R-L$ circuit is denoted as R. The capacitor of the DC-side voltage

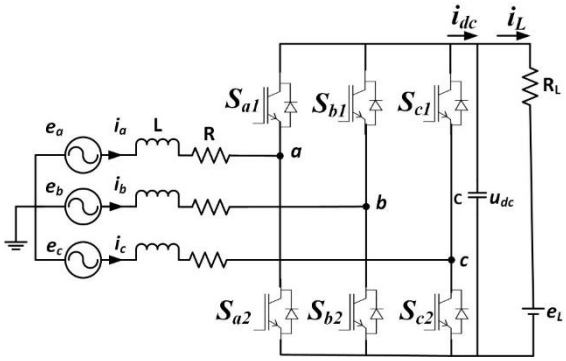

FIGURE 3. 3-Φ bi-directional AC-DC/DC-AC converter.

is denoted as C. The voltage and current of the DC-side are denoted as u_{dc} and i_{dc}, respectively. The load of the DC-side is denoted as R_L and e_L. The system can be explained as stated in equation (1) by considering the line-loop equation of the circuit [33].

$$\begin{bmatrix} e_a \\ e_b \\ e_c \end{bmatrix} = \begin{bmatrix} R & 0 & 0 \\ 0 & R & 0 \\ 0 & 0 & R \end{bmatrix} \begin{bmatrix} i_a \\ i_b \\ i_c \end{bmatrix} + \begin{bmatrix} L & 0 & 0 \\ 0 & L & 0 \\ 0 & 0 & L \end{bmatrix} p \begin{bmatrix} i_a \\ i_b \\ i_c \end{bmatrix} + \begin{bmatrix} v_{ra} \\ v_{rb} \\ v_{rc} \end{bmatrix} \quad (1)$$

To control the output voltage of the rectifier, a vector decoupling sine pulse width modulation (SPWM) control technique is utilized. Fig. 4 shows the rectifier circuit of the three-phase SPWM. Switches of SPWM are denoted as S_a, S_b, S_c. The switches are utilized to set up the linear relationship between the rectifier inputs (v_{ra}, v_{rb}, v_{rc}) and dc bus voltage (v_{dc-bus}). This linear relationship is expressed as mathematically in equation (2) [7].

$$v_{ra} = \frac{S_a.v_{dc-bus}}{2}, \; v_{rb} = \frac{S_b.v_{dc-bus}}{2}, \; v_{rc} = \frac{S_c.v_{dc-bus}}{2} \quad (2)$$

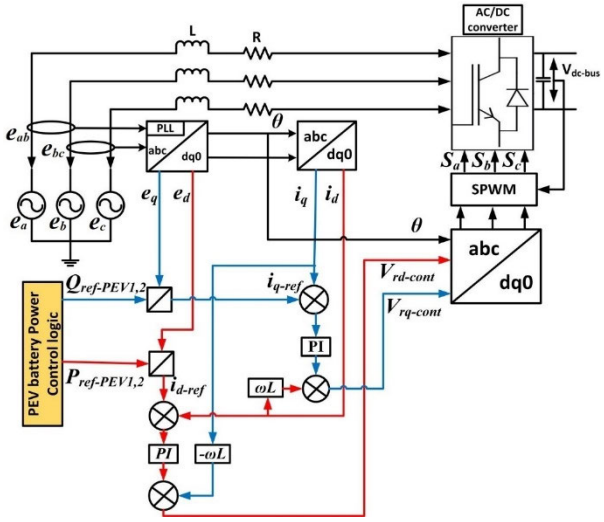

FIGURE 4. Part-A: A bi-directional vector decoupling SPWM rectifier.

After using Park's transformation, the system equation is converted into rotating d-q references and expressed mathematically in equation (3) [7].

$$\begin{bmatrix} e_q \\ 0 \end{bmatrix} = \begin{bmatrix} R + L_p & wL \\ -wL & R + L_p \end{bmatrix} \begin{bmatrix} i_q \\ i_d \end{bmatrix} + \begin{bmatrix} v_{rq} \\ v_{rd} \end{bmatrix} \tag{3}$$

where $v_{rq} = \frac{S_q \cdot v_{dc-bus}}{2}$, $v_{rd} = \frac{S_d \cdot v_{dc-bus}}{2}$

The governing equation of DC output of rectifier referred to DC voltage side is given by the equation (4) [34].

$$C\frac{dv_{dc-bus}}{dt} = \frac{3.S_q.i_q}{2} - \frac{v_{dc-bus}}{R_L} \tag{4}$$

The finalized mathematical model of the prescribed system can be expressed by equation (5) [34].

$$\begin{bmatrix} \frac{di_q}{dt} \\ \frac{di_d}{dt} \\ \frac{dv_{dc-bus}}{dt} \end{bmatrix} = \begin{bmatrix} \frac{-R}{L} & w & \frac{-S_q}{L} \\ w & \frac{-R}{L} & \frac{-S_d}{L} \\ \frac{3S_q}{2C} & 0 & \frac{-1}{CR_L} \end{bmatrix} \begin{bmatrix} i_q \\ i_d \\ v_{dc-bus} \end{bmatrix} + \begin{bmatrix} \frac{1}{L} & 0 & 0 \\ 0 & 0 & 0 \\ 0 & 0 & 0 \end{bmatrix} \begin{bmatrix} e_q \\ 0 \\ 0 \end{bmatrix} \tag{5}$$

An algorithm controls the continuous current flow during the operation of V2G and G2V. Not only the current but also the optimal real power ($P_{ref-PEV1,2}$) exchange is controlled by the algorithm. To ensure the power factor at unity, the reactive power $Q_{ref-PEV1,2}$ is set to zero intentionally. The power balance equation can be written by considering the losses of the system as follows [34]:

$$\frac{3}{2}v_{rq}i_q = v_{dc-bus}C\frac{d}{dt}v_{dc-bus} + \frac{v_{dc}^2}{R_L} \tag{6}$$

PI controllers are utilized to control DC signals and remove steady-state errors because the d-q transformation technique is utilized. These PI controllers are tuned for this purpose. v_{rq}^{cont} and v_{rd}^{cont} voltages are considered as the modulating signals for the SPWM technique. In the d-q frame of references, the grid active and reactive power is calculated as follows [35]:

$$P(t) = \frac{3}{2}(v_{rq}i_q - v_{rd}i_d) \tag{7}$$

$$Q(t) = \frac{3}{2}(v_{rq}i_d - v_{rd}i_q) \tag{8}$$

where $v_{rq} = \frac{S_q v_{dc-bus}}{2}$, and $v_{rd} = \frac{S_d v_{dc-bus}}{2}$.

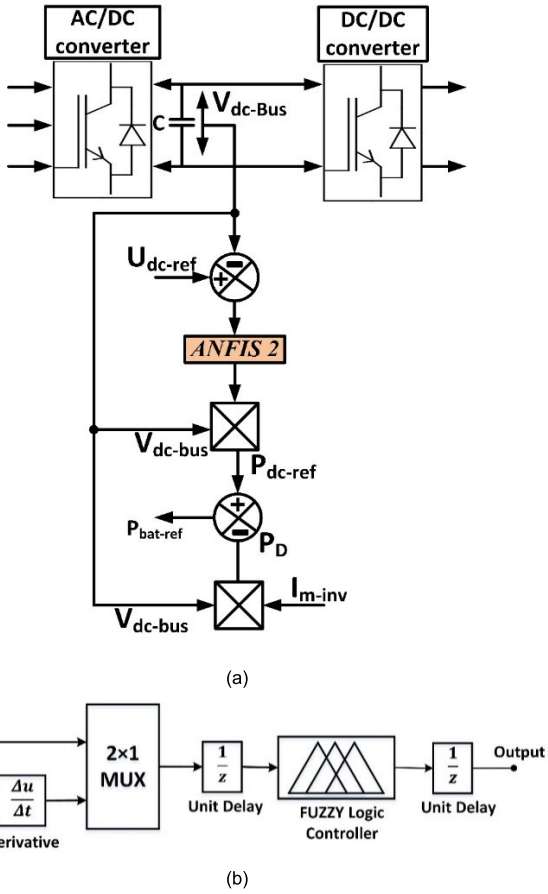

FIGURE 5. Part-B: (a) DC bus voltage controller and (b) internal configuration of ANFIS2 controller in Simulink block.

2) PART-B: DC BUS VOLTAGE CONTROL

This part shown in Fig. 5 (a) demonstrates the control of DC bus voltage along with the ANFIS2 controller where the nominal value of the DC bus voltage is chosen as 400V, and the internal configuration of the ANFIS2 controller is shown Fig. 5 (b). This reference value of DC bus voltage is maintained at any mode of operation like V2G and G2V. The ANFIS2 controller ensures this voltage level during the operation of any direction of power exchange. DC power exchanged ($P_{batt-ref}$) by the battery is calculated from DC bus voltage ($P_{DC-bus-ref}$) and demand power ($P_{Demand-ref}$)

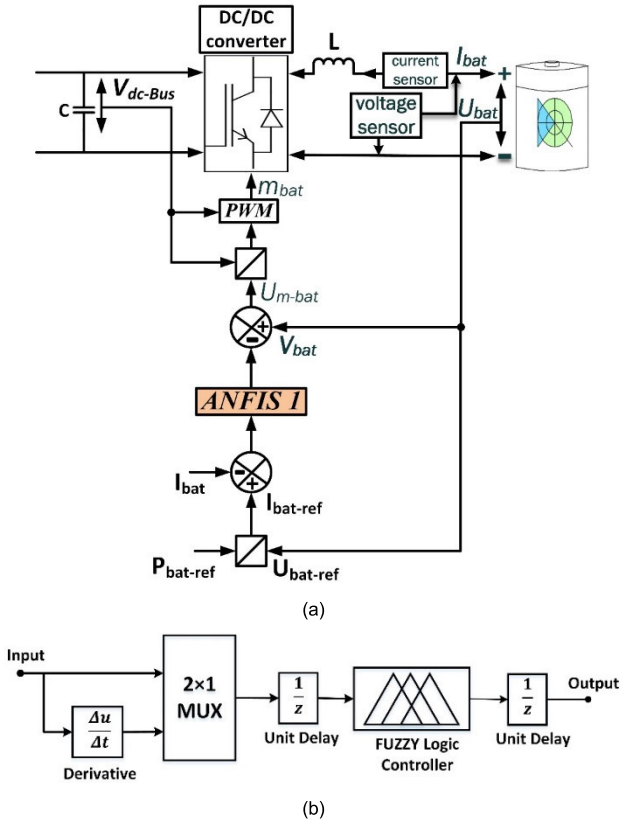

FIGURE 6. Part-C: (a) A bi-directional DC/DC SMPS and (b) internal configuration of ANFIS1 controller in Simulink block.

that can be expressed as follows [16]:

$$P_{batt-ref} = P_{DC-bus-ref} - P_{Demand-ref} \tag{9}$$

3) PART-C: DC/DC SMPS CONVERTER

A fully controlled bi-directional DC-DC switched-mode power supply (SMPS) converter along with ANFIS1 controller is utilized and demonstrated in Fig. 6 (a), and the internal configuration of the ANFIS1 controller is shown in Fig. 6 (b). This converter applies the configuration of switching frequency and sampling rate of 8 kHz and 0.3ms, respectively. This configuration provides the converter with a faster response of detecting any variation of load on either side. This converter also ensures the low total harmonics distortion (THD) and power factor at unity. A capacitor of 1200μF is utilized on the inverter side. This converter also works in current-controlled mode and controls the battery current to have a reference battery current value, $I_{battery-ref}$. Finally, this reference battery current is controlled by the ANFIS1 controller and expressed as follows:

$$U_{m-battery} = U_{battery} - controller\ o/p * \left(I_{battery-ref} - I_{battery}\right) \tag{10}$$

where $U_{m-battery}$ is the modulated voltage of DC/DC SMPS (V), $U_{battery}$ is battery terminal voltage (V), and $I_{battery}$ is the battery current.

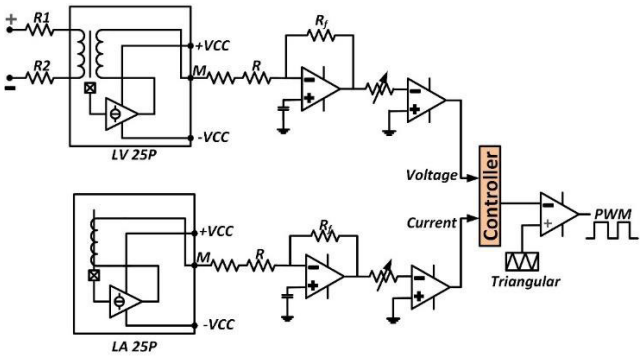

FIGURE 7. Sensing circuit for both voltage and current detection and measurement.

This converter also ensures two major operations such as i) nominal voltage level for battery charging and ii) nominal voltage level for inverter input at unity power factor. The following equation regulated the control of this DC/DC SMPS and expressed as follows:

$$m_{bat,reference} = \frac{U_{m-battery}}{v_{dc-bus}} \tag{11}$$

where $m_{bat,reference}$ is the duty ratio of the controller.

4) SENSING CIRCUIT

This study utilizes a classical sensing circuit model to simultaneously sense the voltage and current, as shown in Fig. 7. The Simulink configuration of the sensing circuit, which is utilized in the grid side, is shown in Fig. 2, senses the voltage and current from the AC power grid and finally converts to a PWM signal with the help of the controller. The sensors connected with the battery input side only sense the battery input voltage and current, and accordingly, give feedback to the controller circuit. The modulation index regulates the output voltage of the converter. The converter voltage is calculated as follows:

$$V_{cc} = \frac{m v_{dc-bus}}{\sqrt{2}} \tag{12}$$

C. BATTERY MODELLING

In this study, the battery part of PEV is considered, which serves the energy storage purpose and also helps in performing V2G and G2V operations. A classical empirical model of the Li-ion battery of PEV is considered. The Li-ion battery model can be explained as a combination of a voltage source and its corresponding resistance, which has been shown in Fig. 8.

For the purpose of G2V and V2G operations, battery function is characterized as charging and discharging mode.

The charging equation is expressed as follows [37]:

$$U_{batt-charge} = U_0 - R \cdot i_k - K \cdot \frac{Q}{i_k \cdot T - 0.1 \cdot Q} \cdot i^* - K \cdot \frac{Q}{Q - i \cdot t} \cdot i_k \cdot T + A \cdot e^{-B \cdot i_k \cdot T}, \rightarrow i^* < 0 \tag{13}$$

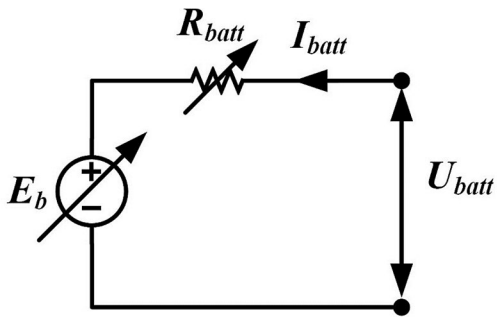

FIGURE 8. A simplified model circuit of a lithium-ion battery [36].

The discharging equation is expressed as follows [37]:

$$U_{batt-discharge} = U_0 - R \cdot i_k - K \cdot \frac{Q}{Q - i_k \cdot t} \cdot (i_k \cdot T + i^*) + A \cdot e^{-B \cdot i_k \cdot T}, \rightarrow i^* > 0 \quad (14)$$

To get the optimal performance of the Li-ion battery, the state of charge (SOC) is a very important parameter in terms of the battery management system (BMS). In this study, the battery SOC level is well maintained within a fixed range to ensure longer battery life. The SOC level is maintained within 20% to 80% for avoiding deep discharging and overcharging. To determine the SOC value of battery Ah method is utilized and expressed as follows [38]:

$$SOC\,(k) = SOC\,(0) - \frac{T}{C_n} \int_0^k (\eta . i\,(t) - S_d) dt \quad (15)$$

where SOC (0) denotes the primary value of SOC, T denotes sampling time, the nominal storage volume is denoted by C_n, η denotes coulombic efficiency, the load current is denoted by $i\,(t)$, and the self-discharging rate is denoted by S_d.

The instantaneous value of the state of charge (SOC) of the battery can be obtained with the following equation [39]:

$$\Delta\,(SOC) = -\frac{i_k \cdot t}{Q_{batt}} \quad (16)$$

The number of series battery cells is calculated as follows [16]:

$$M_{series} = \frac{V_{dc-bus}}{V_{reference}} \quad (17)$$

Parallel battery cell is calculated using the following equation [16]:

$$M_{parallel} = \frac{V_{battery}}{(V_{ref.cel.bat} - \eta_{E-W} \cdot W_{ref.cel.bat}) * M_{series}} \quad (18)$$

where $\eta_{E-W=\alpha \cdot 1,4}$, η_{E-W} denotes the change in energy with respect to weight, and the PEV inclination slope is defined as α.

The state of health (SOH) of the battery cell is calculated as follows [40]:

$$SOH = \min \begin{cases} \left(\frac{R_{max} - R_t}{R_{max} - R_0}\right) & *100\% \\ \left(\frac{C_t - C_{min}}{C_0 - C_{min}}\right) & *100\% \end{cases} \quad (19)$$

where R_{max} is the highest admissible resistance, R_t is the current value of resistance, R_0 is the initial value of resistance, C_0 is the starting volume of capacity, C_t is the current volume of capacity, C_{min} is the minimum tolerable capacity.

III. FIVE STEPS PROPOSED CONTROL STRATEGY FOR PEV POWER MANAGEMENT

A five operational control strategy is considered to ensure optimal power exchange between the power grid and PEV, as depicted in Fig. 9. This control algorithm is applicable for residential houses having two PEVs only. This control strategy identifies the connection status of each PEV and determines the priority vehicle from their connection status. The priority vehicle is determined by analyzing its SOC status. For example, a PEV is available to inject power into the grid, but at the same time, the AC grid also has a surplus of power, so in this circumstance, the priority vehicle will be waiting until the AC grid needs additional power from the PEV. This control algorithm also avoids deep discharging and overcharging of each priority PEV, increasing the battery life to prevent health deterioration. The total power can be calculated by considering the total power of the appliances ($P_{appliances}$) and the total number of PEVs' power ($P_{total-pev}$) utilized at home. So, the total power (P_{total}) is calculated as follows:

$$P_{total} = P_{appliances} + P_{total-pev} \quad (20)$$

The reference average power ($P_{avg.}$) over 24 hours can be calculated as follows:

$$P_{avg.} = \frac{P_{total}}{T_{total}} \quad (21)$$

The amount of power ($P_{diff.}$) that should be injected or absorbed into the AC grid by the PEV can be calculated as follows:

$$P_{diff.} = P_{appliances} - P_{avg.} \quad (22)$$

In every instance of time, the total number of PEV, their connection status/time, the priority vehicle, and the polarity of $P_{diff.}$ are determined. Some important points were considered during the execution of the control logic algorithm:

- First case: If the determined $P_{diff.}$ by equation (22) is negative, then there is a power surplus in the AC power grid and this power should be absorbed by the connected PEV. In this instance, if the SOC value of the connected PEV is greater than or equal to the SOC_{max}, there will be no power exchange between the PEV and AC power grid. Else, if the SOC value of the

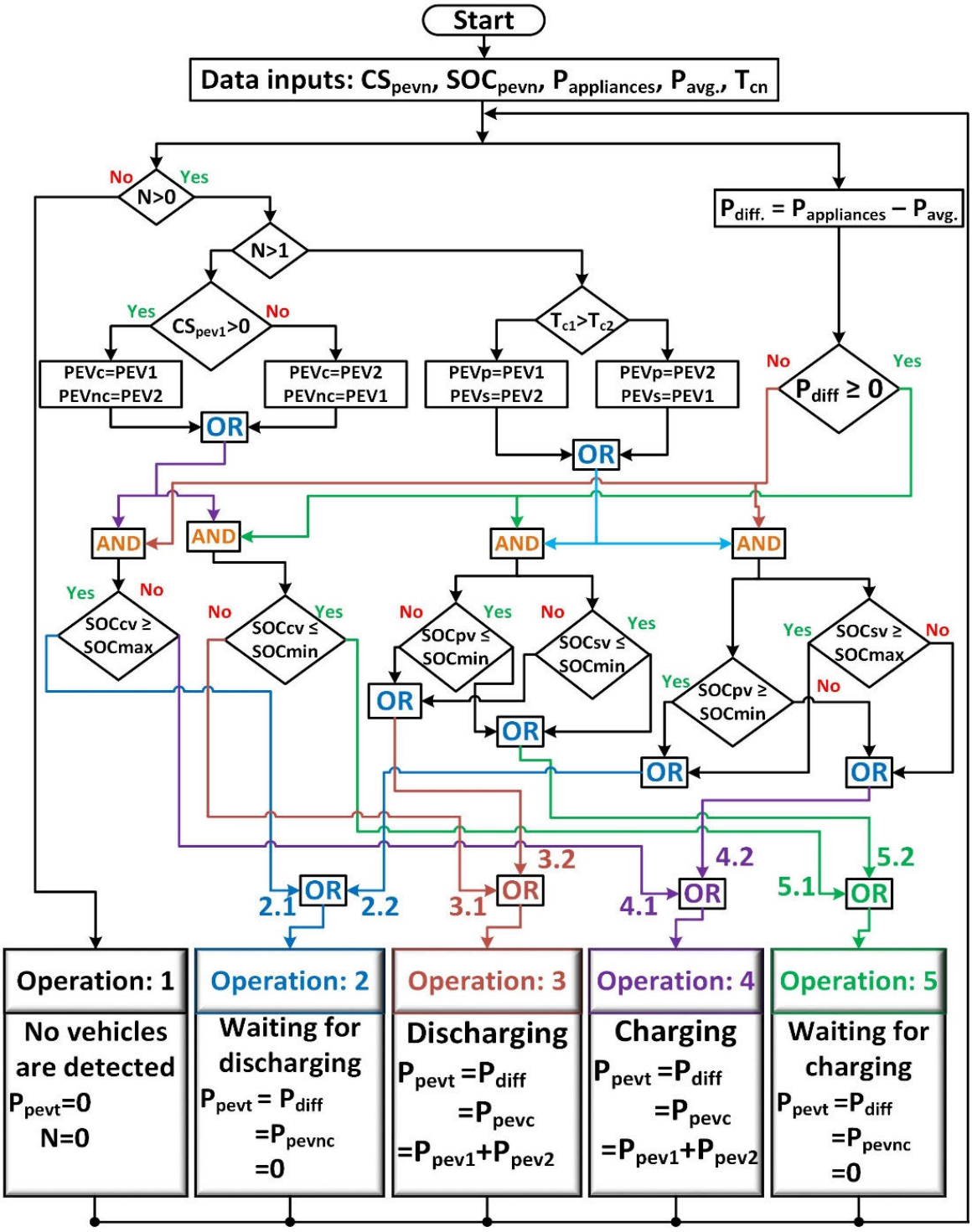

FIGURE 9. Five operations-based control strategies for power exchange between PEV and AC power grid.

connected PEV is less than the SOC_{max} or equal to the SOC_{min} then PEV will start charging until it is fully charged.

- Second case: If the determined $P_{diff.}$ by equation (22) is positive, then there is a power deficiency in the AC power grid and this shortage of power should be supplied by the connected PEV. And this is only possible if the SOC value of the connected PEV is greater than the SOC_{min} or equal to SOC_{max}, unless there will be no power exchange between the PEV and AC power grid if the SOC value of the connected PEV is less than or equal to the SOC_{min}.

Fig. 9 demonstrates that the control strategy initially takes input of connection status of each PEV (CS_{pevn}), SOC status of each PEV (SOC_{pevn}), connection time of each PEV (T_{cn}), total power of home appliances ($P_{appliances}$), and average reference power of total load ($P_{avg.}$). Five operational cases operate the whole control strategy and they have different interactive modes.

A. DIFFERENT INTERACTIVE OPERATIONS OF PEVS

1) OPERATION 1

This mode of operation is enabled when no PEV is connected or the system detects zero PEV. If no PEV is detected, then no power exchange is possible between the PEV and AC power grid. So, the total power exchange is, '$P_{pevt} = 0$'.

2) OPERATION 2

This operational mode is utilized if any of the connected PEV has to wait for discharge. This mode works for two different cases (2.1 and 2.2). In both cases, the $P_{diff.}$ is negative, so any vehicle that connects with the system cannot discharge the power to the system as system has surplus of power, and at the same time the connected PEV is also either fully or partially charged.

Operation case 2.1 is selected by the connected PEV when $P_{diff.}$ is less than zero or has a negative value, and the SOC value of the connected PEV is greater than or equal to SOC_{max}.

Operation case 2.2 is selected when $P_{diff.}$ is negative and the SOC value of the connected priority or secondary PEV is greater than SOC_{min} or equal to SOC_{max}, respectively.

So, for both cases, the total power exchange between the PEV and AC power grid is zero ($P_{pevt} = 0$).

3) OPERATION 3

This operational mode is executed when a PEV needs to inject power into the AC grid system. In this mode, $P_{diff.}$ has a positive value, implying that the AC grid needs additional power to drive the extra load during the peak hour. Two cases (3.1 and 3.2) are executed for this operational mode.

Case 3.1 is detected by a connected PEV whose SOC value is greater than SOC_{min}. At the same time, case 3.2 determines which PEV is the priority vehicle along with their SOC level. The detected SOC value of the connected priority or secondary PEV is greater than SOC_{min}. For both cases, the selected PEV is ready to inject power into the AC grid. It keeps executing this operational mode until it is fully discharged or gets instruction from another operational mode in the next instance of time. So, in this operational mode, total power exchange is calculated to be '$P_{pevt} = P_{pev1} + P_{pev2}$'.

4) OPERATION 4

The charging process is executed by the operational mode 4. This operational mode is also segregated into two different cases (4.1 and 4.2). For both cases, the $P_{diff.}$ is negative and any PEV with SOC_{min} is connected with the system that can take power from the AC grid.

For case 4.1, if the only one connected PEV has a SOC value less than SOC_{max}, then it can start charging until the current operation is executed or get the next operational instruction.

Case 4.2 is executed when two PEVs are connected, and a priority vehicle is selected from the connected PEVs. If any of the connected priority or secondary vehicles have a SOC value equal to SOC_{min} or less than SOC_{max}, then the connected PEV will start charging.

The total power exchange between the PEV and AC power grid for this operational mode will be '$P_{pevt} = P_{pev1} + P_{pev2}$'.

5) OPERATION 5

This operational mode works as opposite of operational mode 2. This operational mode provides the connected or priority vehicle to keep waiting until it gets the opportunity to start charging or get fully charged. Like other operational modes, this operational mode is also the combination of two different cases (5.1&5.2). For this operational mode, the calculated $P_{diff.}$ is positive.

Case 5.1 is a standalone case where the connected PEV has a SOC value greater than or equal to SOC_{min} but still, it cannot start charging as the $P_{diff.}$ is positive.

Case 5.2 is executed when two PEVs are connected simultaneously with the system. From the connected PEVs, the priority or secondary vehicle is determined where either of the connected PEV has a SOC value equal to SOC_{min}.

Thus, in this operational mode, the power exchange between the PEV and AC grid is zero ($P_{pevt} = 0$).

IV. ANFIS CONTROLLER DESIGN

This study uses a non-linear biogeography-based optimization algorithm to produce the optimum data sets for the ANFIS controller. Fitness criteria are typically used in intelligent searching processes to evaluate the many individuals confronted while the course is executing.

A. BIOGEOGRAPHY-BASED OPTIMIZATION (BBO) PROCEDURE

The BBO, being an occupant-based calculation, looks through a technique that requires a number (NP) of competitor arrangements (X_d^n) called natural surroundings to shape a generation (P^n), wherein every living space would contain certain arrangement highlights (SIV_{nd}). The algorithm is based on the following steps:

1) STEP-1: INITIALIZATION

The free choice factors in BBO strategy ordinarily, called SIV_s, are control boundaries needed to be optimized while limiting or expanding a fitness index. A real-valued vector of SIV_s defines a habitat or island. The problem dimension decides the number of SIV_s in a habitat. For the optimization problem, each habitat in the population is a potential solution.

The largest amount of species S_{max}, the highest emigration E, immigration rates I, the elitism parameter p, and the highest mutation rate m_{max} are among the BBO parameters used. The number of generations'n, the problem size d, the length of each control element SIV, and the population numbers NP are all defined.

For each control variable SIV, the first inhabitants are randomly created inside the search space based on the relationship.

$$x_{k,i}^{n} = x_{i,min}^{n} + random\left(x_{i,max}^{n} - x_{i,min}^{n}\right) k = 1, NPi = 1, d \tag{23}$$

2) STEP-2: EVALUATION OF FITNESS

The appropriateness indices are calculated by evaluating the objective function once the initial solutions have been formed. The fitness criteria are computed using the following equation after the composite non-linear system model is generated after incorporating a P-Q decoupled control-based energy storage system.

$$J = min\left\{\int_{t=0}^{tsim} t\left[\alpha_1 \left|d\omega\right| + \alpha_2 \left|dV_s\right| + \alpha_3 \left|dV_{dcs}\right|\right] dt\right\} \tag{24}$$

The HSI is mapped with several essential elements such as the population count S, emigration rate μ, and immigration rate λ using the following relation.

$$\lambda_i = I\left(\frac{1-n_i}{m}\right) \text{ and } \mu_i = E\left(\frac{n_i}{m}\right) \tag{25}$$

The best solution is regarded as the habitat with the highest fitness value, and the optimum outcome is updated for each generation by storing it in an additional factor.

3) STEP-3: ELITISM OPERATION

In terms of HSI values, rank the population in the order of appearance. A predetermined p number of superior habitats are transmitted down to the following generation unchanged.

4) STEP-4: MIGRATION PROCESS

The non-elite response members are then stochastically moved to better locations. The technique for choosing any SIV for relocation is outlined below:

a. The lower immigration rate λ_{lower} and the upper emigration rate μ_{upper} are chosen for a certain population set.
b. The real immigration λ and emigration rates μ for each island are calculated.
c. Following that, habitat and SIV based on that rates are chosen.

In BBO, the migratory method makes a population group distinct from the initial collection of habitats.

5) STEP-5: MUTATION PROCESS

The relation is used to update the number of species likelihood for each island.

$$\frac{dP_S}{dt} = \begin{cases} -\left(\lambda_i + \mu_i\right) P_S + \mu_{i+1} P_{S+1} & S = 0 \\ -\left(\lambda_i + \mu_i\right) P_S + \mu_{i+1} P_{S+1} & \\ \quad +\lambda_{i-1} P_{S-1} & 1 \le S \le S_{max} - 1 \\ -\left(\lambda_i + \mu_i\right) P_S + \lambda_{i-1} P_{S-1} & S = S_{max} \end{cases} \tag{26}$$

Then, depending on their probability, each of the non-elite habitats goes through a mutation process. Habitats with mutation rates greater than a randomly generated number are chosen for mutation, as estimated from equation (27). The current habitat set is replaced with a randomly created island set, giving population diversity. Each new island set's fitness index is calculated.

$$mt = m_{max} * \left(\frac{1 - P_i}{P_{max}}\right) \tag{27}$$

Here, P_{max} is the greatest species count probability, while m_{max} is a user-defined value.

6) STEP-6: STOPPING CRITERIA

When the following conditions are met, the iterative process comes to an end.

a. The total number of generations has been reached.
b. The number of generations in which a solution remains unchanged exceeds a specified threshold.
c. A suitable solution is found.

The different steps that make up the BBO algorithm's optimization technique are depicted in Fig 10.

B. ANFIS CONTROLLER MODELING

A fuzzy toolbox in MATLAB is used to design ANFIS. It has features including fuzzy inference system (FIS), MF for input and MF for output, rules viewer, and output surface. The user defines the number of MFs and their range, and they are changeable. ANFIS uses Sugeno, which gives the flexibility in changing the MFs and their range. Training of different frameworks is done by reverse approach or combined reverse approach and minimum square approach technique. Total deviation and square of real and expected output help to calculate different frameworks and this process is known as the optimization technique. The main privileges of using ANFIS are time effectiveness and the least effortless. ANFIS does not need human expert knowledge; hence it consumes the least time and is more straightforward in parameter selection and MFs optimization, thus contributing to sustainability.

The ANFIS framework works in two commonly particular stages: the neural-network stage, where the framework orders information and discovers designs. The other stage fosters a fuzzy master framework through versatile tuning of participation capacities. A fuzzy inference system (FIS) file is generated by utilizing data pairs of input and output.

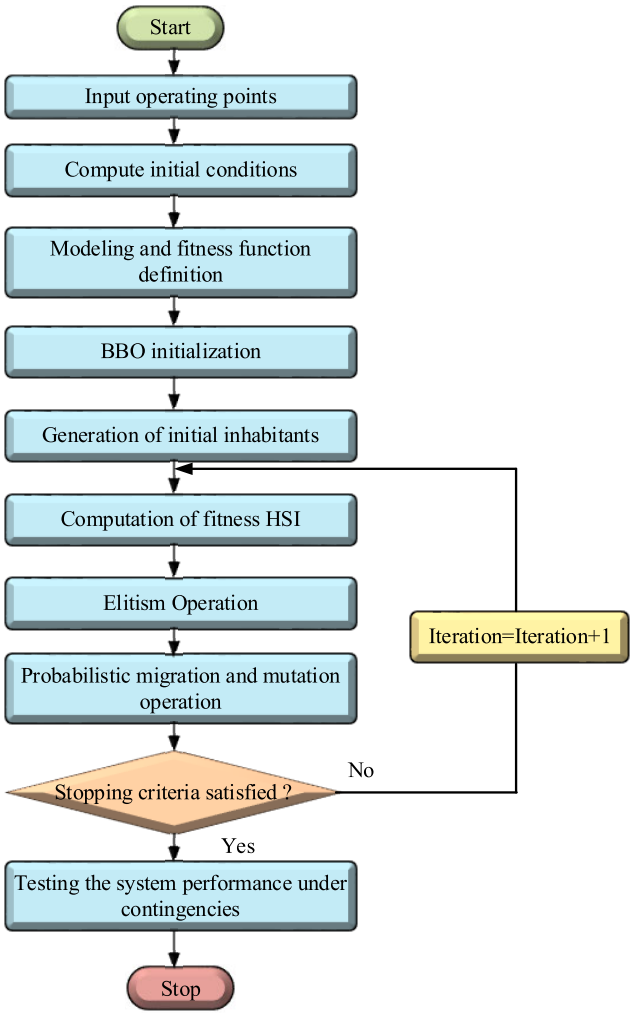

FIGURE 10. Flow chart of a BBO-based optimal control design.

At the same time, tuning of membership functions is carried out with the help of either the least-squares method or a backpropagation algorithm or a combination of both. For the ANFIS, the input parameters are known as linear parameters and the output parameters are known as non-linear parameters. Two fuzzy input based if-then rules form the knowledge foundation for this system and are given by the following equation:

$$if\ e\ is\ A_i\ and\ \Delta e\ is\ B_i\ then\ f_i = p_i e + q_i \Delta e + r_i \quad where\ i = 1, 2 \qquad (28)$$

Ai and Bi denote the linguistic variables while the output function is f_i and the linear parameters of i^{th} rules are p_i, q_i and r_i.

The ANFIS architecture shown in Fig. 11 constitutes of five layers; the output of every layer is denoted by $L_{l,i}$, where l represents the layer number and i represents the neuron number. The detailed explanation of each layer is as follows:

1) LAYER 1

This layer is utilized to fuzzify non-linear input with the help of linguistic variables like small, medium, large etc. The output of this layer is determined with the use of membership functions stated in these linguistic parameters. In this layer, the parameters are known as non-linear parameters and the node i stated as an adaptive node. The mathematical expression of each node is as follows:

$$\begin{aligned} L_{1,i} &= \mu_{A_i}(e), \quad \text{where } i = 1, 2 \ldots\ldots j \\ L_{1,i} &= \mu_{B_i}(\Delta e), \quad \text{where } i = 1, 2 \ldots\ldots j \end{aligned} \qquad (29)$$

where e and Δe denote the deviation and change in deviation, respectively and are used as inputs for node i. $\mu_{A_i}(e)$ *and* $\mu_{B_i}(\Delta e)$ address the membership functions that build up how much the given data sources e and Δe fulfils the quantifier A_i and B_i. For each node, the membership functions are allotted by Gaussian membership function, which is expressed as follows:

$$\mu_{A_i}(x) = exp\left[\frac{-1}{2}\left(\frac{x - c_{ij}}{\sigma_{ij}}\right)^2\right] \qquad (30)$$

where c_{ij} denotes the mean and σ_{ij} denotes the variance of the jth function. The mean and variance are known as non-linear parameters, and they are adapted during the learning procedure of ANFIS.

2) LAYER 2

Firing strength for each standard evaluating how much information has a place with that standard is figured in this layer. This node is denoted as P, and this layer's output is determined from the multiplication of all incoming signals. The node function for this layer is expressed mathematically as follows:

$$L_{2,i} = \mu_{A_i}(e) * \mu_{B_i}(\Delta e), \quad \text{where } i = 1, 2 \qquad (31)$$

3) LAYER 3

Normalization operation is performed by the nodes which are presented in this layer. These nodes are known as fixed nodes and represented as a circle labelled N. The output of this layer node is calculated by taking the ratio of i^{th} rule's firing strength to the sum of all rule's firing strengths. The node function of this layer is presented as follows:

$$\begin{aligned} L_{3,1} &= \bar{w_1} = \frac{w_1}{w_1 + w_2} \\ L_{3,2} &= \bar{w_2} = \frac{w_2}{w_1 + w_2} \end{aligned} \qquad (32)$$

4) LAYER 4

The node in this layer is recognized as an adaptive node. The function of this node is expressed as follows:

$$\begin{aligned} L_{4,1} &= \bar{w_1} f_1 = \bar{w_1}(p_1 e + q_1 \Delta e + r_1) \\ L_{4,2} &= \bar{w_2} f_2 = \bar{w_2}(p_2 e + q_2 \Delta e + r_2) \end{aligned} \qquad (33)$$

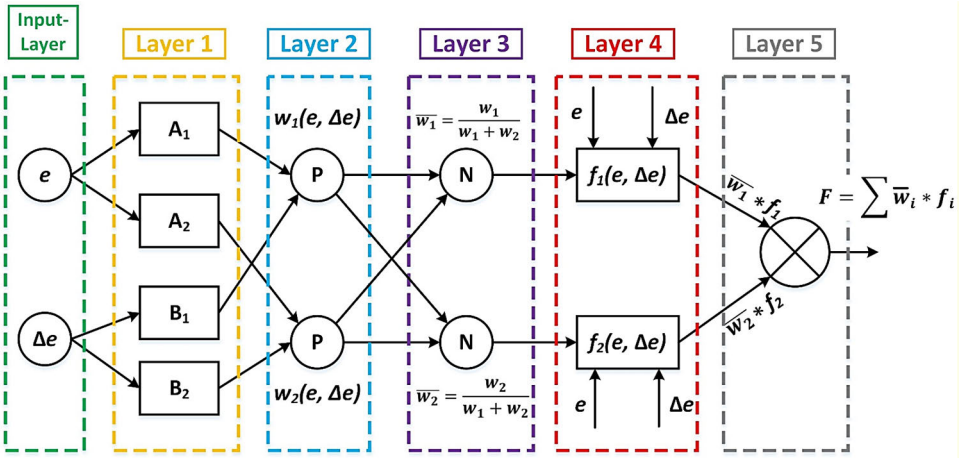

FIGURE 11. Typical equivalent ANFIS architecture.

where $\bar{w}_i$ presents the normalized firing strength. The linear parameters (p_i, q_i and r_i) presented in equation (33) are adjusted by the training process of ANFIS.

5) LAYER 5

The summation of all approaching signals is taken as the general yield of the fifth layer. This layer is named as output layer, which holds a single node and is represented as a circle node with node function as given below:

$$L_{5,i} = \frac{\sum_{i=1}^{2} w_i f_i}{\sum_{i=1}^{2} w_i} \tag{34}$$

To update the different parameters of Layer-2 (non-linear) and Layer-4 (linear) hybrid algorithm is utilized. The steepest descent method and least-square method are associated as hybrid algorithms of ANFIS parameters. Forward propagation and backward propagation are mainly two propagation processes followed by this hybrid algorithm. Using the forward propagation method, the output nodes are forwarded up to Layer-4. The least-square method helps synthesize the linear parameters. By utilizing the backpropagation method, the error data is propagated backwards. The gradient descent method helps synthesize the non-linear parameters. Compared to the conventional backpropagation algorithm, the convergence speed of the hybrid algorithm is faster because, during the training process, the search space dimensions are minimized effectively.

In this study, two ANFIS controllers are designed to carry out simulations as well as analyze the results. ANFIS1 is designed to control the PEV's battery current, while ANFIS2 is designed to control the bus voltage to a nominal DC value for the battery input. These two controllers ultimately control the battery power. Both controllers utilize two input variables for better preciseness, such as deviation (e) and change in deviation (Δe). The output is also regulated to achieve better results. The deviation is measured from the difference between practical and standard/reference values; change in deviation is measured from the ratio between the difference values and standard values.

The data set for ANFIS1 is produced by equations (35) and equation (36). For data set production, equation (35) and equation (36) are provided as input variable 1 (e) and input variable 2 (Δe) of MF, respectively, in the fuzzy toolbox. In this way, the primary FIS file for ANFIS1 is generated for training purposes. Equation (35) calculates the deviation of battery current and is as follows:

$$U_{m-battery} = U_{battery} - controller\ o/p * \left(I_{battery-ref} - I_{battery}\right) \tag{35}$$

where $U_{m-battery}$ is the battery voltage level after the modulation, $U_{battery}$ is the voltage level of battery which is taken from battery ratings and the value is 400V, $controllero/p$ stands for Controller output, $I_{battery-ref}$ denotes the battery reference current, which is taken from battery ratings, and $I_{battery}$ represents the practical battery current without an ANFIS controller.

Equation (36) calculates the change in deviation of battery current and is as follows:

$$Changein\ battery\ current\ deviation = \frac{\left(I_{battery-ref} - I_{battery}\right)}{\left(I_{battery-ref}\right)} \tag{36}$$

The data set for ANFIS2 is produced by equations (37) and equation (38). For data set production, equation (37) and equation (38) are provided as input variable 1 (e) and input variable 2 (Δe) of MF, respectively, in the fuzzy toolbox. In this way, the primary FIS file for ANFIS2 is generated for training purposes. Equation (37) calculates the deviation of DC bus voltage and is as follows:

$$Deviation\ in\ DC\ busvoltage = v_{\mathrm{dc-ref}} - v_{dc-bus} \tag{37}$$

where $v_{\mathrm{dc-ref}}$ is the reference DC bus voltage level, which is 400V and v_{dc} is the practical (actual) DC bus voltage level which is considered before utilizing ANFIS controller.

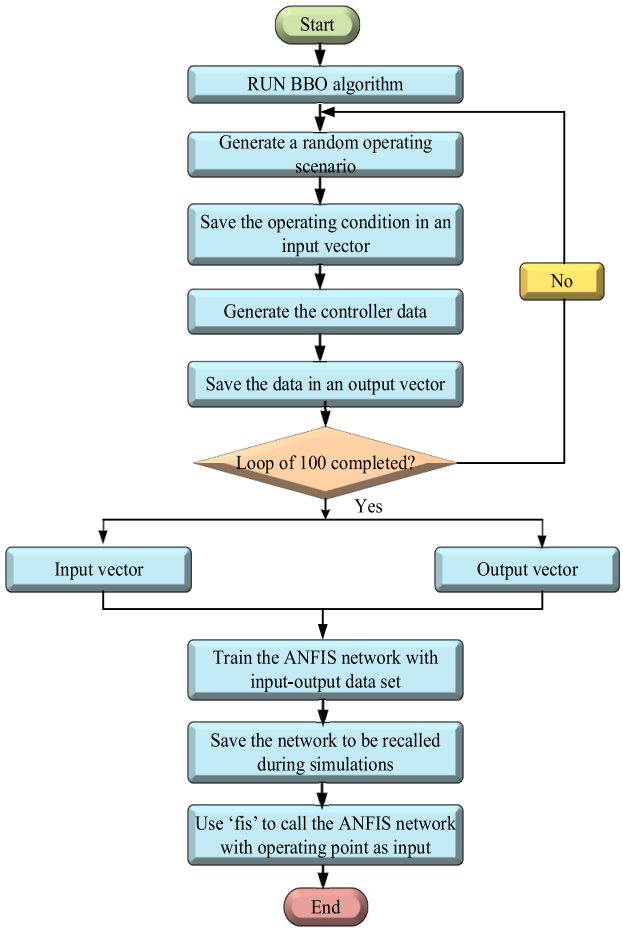

FIGURE 12. Flow chart of ANFIS data training execution process.

Equation (38) calculates the change in deviation of DC bus voltage and is as follows:

$$\textit{Change in deviation in DC bus voltage} = \frac{\textit{Deviation in DC bus voltage}}{(v_{\mathrm{dc-ref}})} \tag{38}$$

C. IMPLEMENTATION OF ANFIS CONTROLLER SCHEME

In this study, a duplicate model of bi-directional power flow between AC power grid and PEVs battery system is modelled using PI controllers by replacing the ANFIS controllers. ANFIS is trained with two inputs, such as deviation (e) and change in deviation (Δe) and single output such as error correction data is produced. The ANFIS network requires training data, which is generated via the BBO algorithm. The procedure begins with creating BBO parameters and the production of random operating conditions, as shown in Fig 12. This input vector is saved in an array on the outside. The approach then uses migration, mutation, and elitism operations to find the best-decoupled controller parameters. The training input-output data pair is generated after executing a cycle of 100 epochs. The adaptive neuro-fuzzy network is then trained and tested as the next phase in the algorithms. The data set is uploaded into the ANFIS platform, and the training process is completed using a hybrid learning algorithm with 500 epochs. The system is preserved for use in simulations that need online controller output computation. The BBO guides the search process with a non-linear fitness function by utilizing equation (24). The set of controller output that achieves the lowest objective value for a given set of beginning conditions are the optimum parameters as we consider error correction for this study. The number of habitats and iterations were set at 50 and 80, respectively. Table 1 lists the BBO technique's additional parameters.

The least-squares procedure helps to find the conforming framework. Any inaccurate number that is greater than the specified standard must be renewed.

The ANFIS toolbox in MATLAB allows a user to upload data, train data, save a new FIS file, and open the final FIS file. To start with ANFIS toolbox, the first action is gathering the training data set. The data bundle is used as an input value for the ANFIS toolbox, and the data bundle should be structured as in matrix format. The matrix's end column is considered the output column, and other than the output column, all columns are considered as input columns. The matrix may have multiple columns as required by the system.

ANFIS training process starts with the creation of a primary membership function. The final membership functions are created at the end of the training process. To increase the data precision, the training data bundle is compared with consisting of the data bundle.

Again, 80 input-output data samples were taken for the learning phase, while the remaining 20 were used to test the network. The considered input characteristics are deviation and change in deviation, and output characteristic is regulated by ALC (Adapted Learner Content).

The process of the ANFIS system is introduced with all built-in values like 7*7 membership functions. There are 180 statements/rules for the fuzzy system, and each of them is generated by ANFIS algorithm and is linear by default. To compensate for the inaccuracy and establish the linkage between the input and output, the whole training data bundles are gone through the ANFIS network. The following is used to observe the training inaccuracy.

$$\textit{Root Means Square Error (RMSE)} = \sqrt{\frac{1}{M}\sum_{k=1}^{M}\left(y_n - \hat{y}_n\right)^2} \tag{39}$$

Mean Average Error (MAE) is used and defined as Mean

$$\textit{Average Error (MAE)} = \frac{1}{M}\sum_{k=1}^{M}|y_n - \hat{y}_n| \tag{40}$$

where M is the total forecasting number, $\hat{y}_k$ is forecasted string, and y_k is the reference string.

Overfitting is a common problem in ANFIS model building, which occurs when the data set is over-trained

TABLE 1. The BBO algorithm parameters.

Parameter description	Value
Population size	50
Iterations	80
Elitism parameter	4
Number of SIV parameters	8
Habitat modification probability	1.0
Lower bound for immigration probability	0
Upper bound for immigration probability	1.0
Step size for numerical integration of probabilities	1.0
Maximum immigration rate I	1.0
Maximum emigration rate E	1.0
Stop iterations	75

by ANFIS. To avoid the overfitting problem, the model is tested by setting a training epoch. The optimization for this study is achieved with the help of selecting optimized MFs, and optimized MFs are achieved by the training process of ANFIS. The sustainability of this study is achieved by establishing a relationship between non-linear input variable 1 and non-linear input variable 2, and the ANFIS training algorithm establishes this relationship.

V. RESULTS AND DISCUSSIONS

To justify the effectiveness of an ANFIS controller, simulation of a PEV's battery charging and discharging with control strategy was accomplished using MATLAB/Simulink and compared with a traditional PI controller.

In this paper, two PEVs are considered: PEV1 is for one person, and PEV2 is for another person from a single-family. The charging/discharging takes place at home parking only. The daily load profile considered in this study is based on real-life power consumptions by different loads at home, and PEV charging/discharging is managed technically to improve the load curve. The battery size of PEV1 is 14 kWh and PEV2 is 11 kWh. For both batteries, the maximum and minimum SOC levels are considered respectively 0.8 and 0.2. Each PEV can inject a maximum of 1.5 kW into the system, and the maximum power that the PEV can take from the system is -1.5 kW.

To justify the whole mechanism, a full-day simulation was conducted. The 24 hours were divided into small fractions of 15 minutes each to get 96 time periods/intervals over 24 hours. So, during any time interval, to perform V2G or G2V operation depends on some parameters like SOC level of the battery, system power demand (peak or off-peak hour), connection time of each PEV and availability of each PEV at home parking. Charging/discharging of each PEV will initiate at the beginning of every time interval and stop at the end of the same time interval.

In this study, PEV's battery is utilized, so the battery is not always available at home. Though two PEVs are used, so the number of batteries is also two. Two modes of power operations are utilized, and these operations help to get optimum use of the battery. These two operating modes are V2G and G2V. Though PEVs are also used for transportation purposes, they are always not available at home, but they are always connected with the system when they are available at home.

A. DIFFERENT INTERACTIVE CASES OF PEV1

Different interactive cases of PEV1 with an AC power grid can be demonstrated from its SOC characteristics curve, as shown in Fig. 13 (a). During the following periods [0, 4 h], [12:30, 14:30 h], [20, 21 h] and [22, 24 h] the PEV1 performs the G2V operation. During these periods, PEV1 charges and tries to achieve its SOC at maximum level (0.8). V2G operation is performed during the periods [6, 7:30 h], [18, 18:40 h] and [21, 22 h] and, at the end of any period, PEV1 may achieve its SOC at the minimum level (0.2). In the periods [4, 6h] and [18:40, 20h], the curve is flattened and parallel to the x-axis, which means PEV1 is still connected to the grid, but it is not performing any operation (inactive). The reason behind the PEV's inactiveness is that before the time interval [4, 6h], the SOC value of PEV1 has already reached its maximum level, and the system also does not require any extra power from the battery.

Again, before reaching the period [18:40, 20h], the SOC value of PEV1 is already reached its minimum level, though, during this period, the system requires additional power from the battery, but PEV1 cannot provide because of its lowest SOC value. During the time intervals [7:30, 12:30h], and [14:30, 18h], PEV1 is used for transportation purposes that is why it is not available at home.

B. DIFFERENT INTERACTIVE CASES OF PEV2

Different interactive cases of PEV2 with AC power grid can be illustrated from its SOC characteristics curve, as presented in Fig. 13 (b).

G2V operation is performed by PEV2 during the time intervals [0, 5:30h], [8:30, 10:30h], [12:30, 14:30h], [20, 21h], and [22, 24h]. PEV2 tries to achieve its higher SOC value during the above-mentioned time intervals.

Discharging time interval is [6, 8:30h], and PEV2 gets its lower SOC value during this period. During this time interval, PEV2 performs the V2G operation.

During the following time intervals [5:30, 6h], [10:30, 11h], [17, 20h], and [21:30, 22h] PEV2 does not do any operation but still it is connected to the system. During these time intervals, it presents a flattened curve and parallel to the x-axis.

In the following periods [11, 12:30h], [14:30, 17h], and [21, 21:30h], PEV2 is used for transportation purposes; that is why it is not available at home.

C. EXPLANATION OF DIFFERENT CHARACTERISTICS CURVES OF PEVS' BATTERY

In this study, the simulation is carried out basically to show the performance of PI and ANFIS controllers in terms of battery characteristics curves. The analyses of Fig. 14, 15, and 16 represent a clear difference in the battery characteristics curves by using PI and ANFIS controllers. To differentiate between the PI and ANFIS controller,

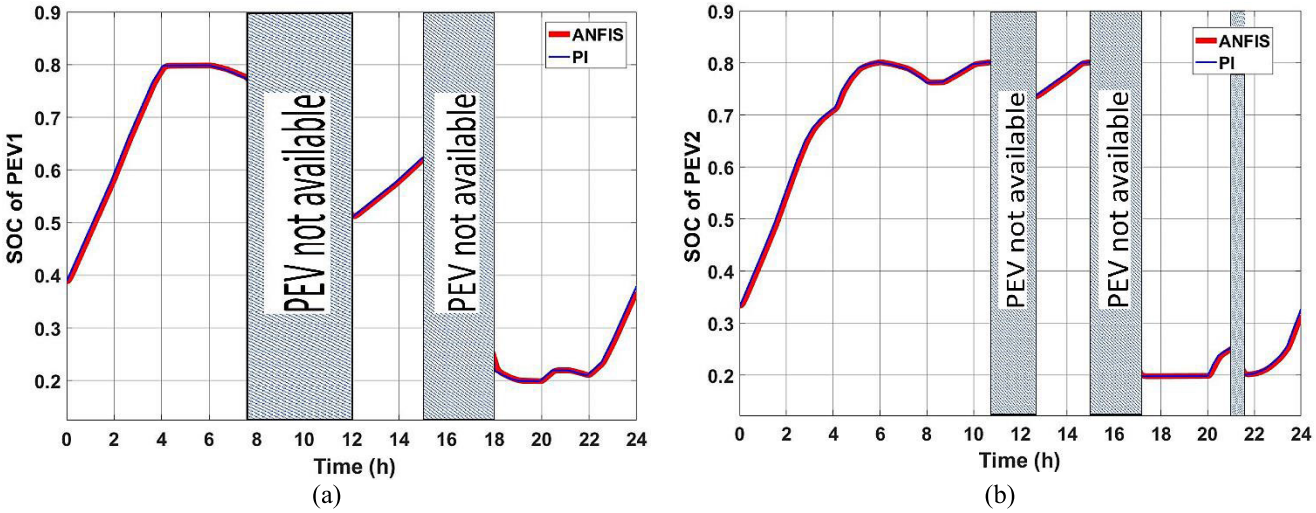

FIGURE 13. SOC wave shape of (a) PEV1 with PI and ANFIS controller and (b) PEV2 with PI and ANFIS controller.

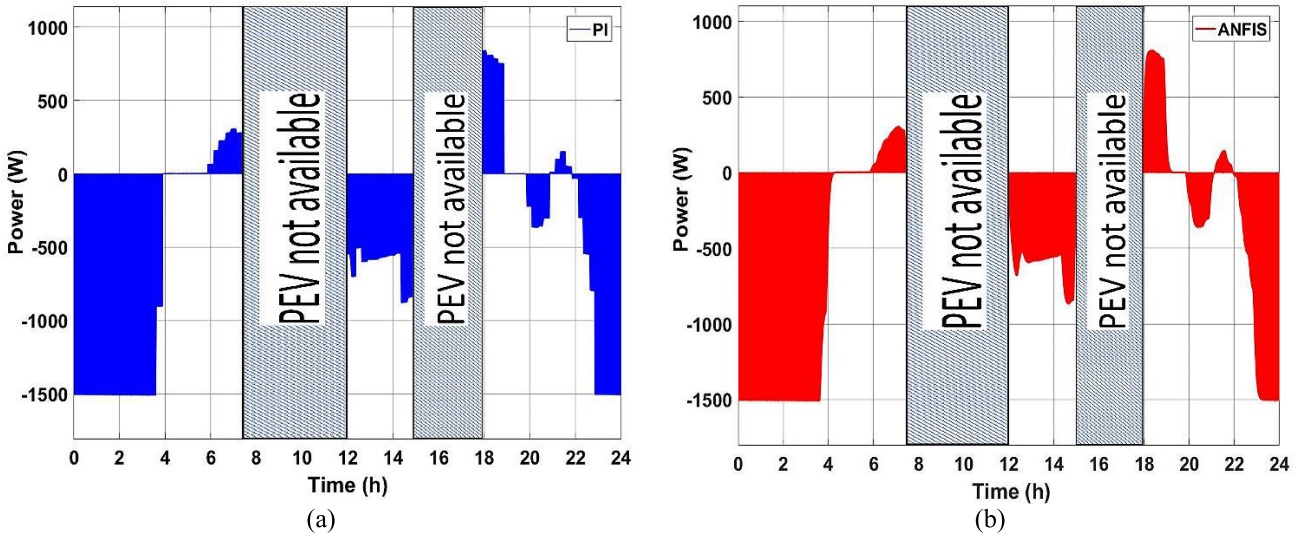

FIGURE 14. Charging profile of (a) PEV1 with PI controller and (b) charging profile of PEV1 with ANFIS controller.

different characteristics curves of PEVs battery have been explained as follows:

1) CHARGING/POWER PROFILE CURVES

The charging profile of PEV1 is depicted in Fig. 14 (a) (with PI controller) and Fig. 14 (b) (with ANFIS controller), while for PEV2, it is displayed in Fig. 15(a) (with PI controller) and Fig. 15 (b) (with ANFIS controller). Here, the charging profiles are considered to explain the different operating modes and their availability at home. In Figs. 14 and 15, the -ve power defines the G2V operation (charging), +ve power defines V2G operation (discharging), 0 (zero) power defines the PEV is still available at home but not exchanging any power, and its unavailability at home is marked in the respective figures.

The rising and falling trend are smoother in Fig. 14 (b) than Fig. 14 (a). From the time interval 6 to 7:30h, the rising trend in Fig. 14 (b) is smoother than the rising trend in Fig. 14 (a). Moreover, the falling trend in Fig. 14 (b) during the time interval 22 to 24h is much smoother than it is shown in Fig. 14 (a). The same analysis also can be carried out for PEV2 by comparing the charging profile in Fig. 15 (a) and Fig. 15 (b).

2) CURRENT PROFILE CURVES

Suppose the battery current curve is considered (Fig. 16 (a) and Fig. 16 (b)) for the comparative analysis. In that case, it is even clearer to justify the benefits of using the ANFIS controller over the PI controller. For PEV1, in Fig. 16 (a), the blue line represents the current curve of the PI controller, and the red line represents the current curve of the ANFIS controller. In Fig. 16 (a) it can be seen that in the case of the PI controller, there is a sudden and large spike at the start, which is removed by using the ANFIS controller

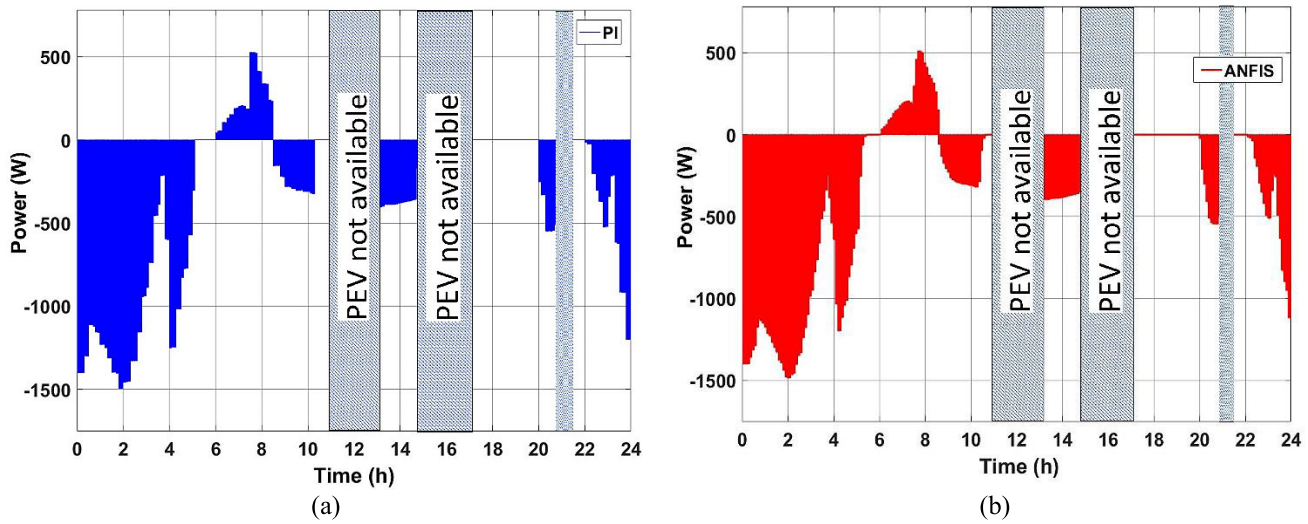

FIGURE 15. Charging profile of (a) PEV2 with PI controller and (b) charging profile of PEV2 with ANFIS controller.

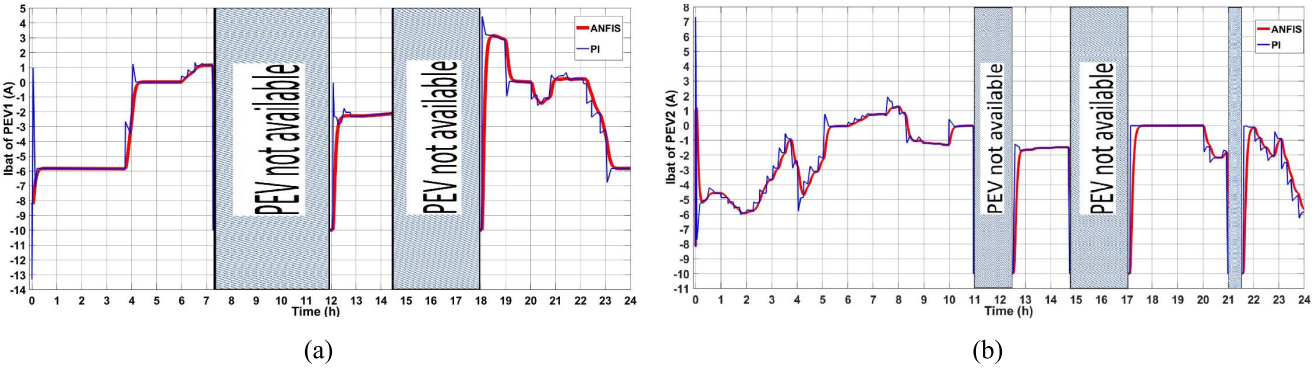

FIGURE 16. Current wave shape of (a) PEV1 with PI and ANFIS controller and (b) PEV2 with PI and ANFIS controller.

TABLE 2. Research summary.

Figure	Period	PI controller	ANFIS controller
16 (a)	[0, 4 h]	Transient instability, ranging from -13.5A to 1A	Smooth transition and stable at -6A
	[4, 6h]	Distorted transition from -6A to 1A and stable at 0A	Smooth transition from -6A to 0A and stable at 0A
	[6, 7:30 h]	Distorted transition from 0A to 1A and stable at 0A	Smooth transition from 0A to 1A and stable at 1A
	[12:30, 14:30 h]	Started charging with transient instability	Smooth transition and stable at -2A
	[18, 24 h]	Again, started charging with transient instability and distortion in every rising and falling period	No transient instability during charging start up and smooth transition in every rising and falling period
16 (b)	[0, 1h]	Transient instability during charging start up, ranging from -8A to 7.5A and stable at -4.5A.	No transient instability is observed.
	[1, 11 h]	Overshoot is observed during every operation of V2G and G2V.	Every operation of V2G and G2V is smooth and no overshoot is observed during any transition of operation.
	[12:30, 14:30 h]	Steady state operation at -1.5A and with startup transient instability.	No transient instability and stable at -1.5A.
	[17, 21 h]	No startup transient instability but overshoot is observed during G2V operation	No transient instability is observed and G2V operation is smooth
	[21:30, 24 h]	No startup transient instability but overshoots are observed during G2V operation	No transient instability is observed and G2V operation is smooth

because the current curve has a smoother increase without any unexpected spikes when using the ANFIS controller. At the beginning of time 12hr and 18hr, the same improvement is observed using the ANFIS controller. Again, during the falling time interval [22, 24h], there are many ripples in the PI controller, which are also eliminated by using the ANFIS controller.

From Fig. 16 (a), it can be stated that the unexpected spikes and all the ripples from the PI controller have been removed by utilizing the ANFIS controller.

The same analysis also can be carried out for PEV2 by comparing the current profile in Fig. 16 (b). The reason for getting a smoother curve using the ANFIS controller is that the ANFIS controller can store previous data; by trial & error method, it learns from the system and finally provides a better result for the next step.

D. RESEARCH SUMMARY

A research summary can be carried out for a better understanding of the objective of this study. To have the research summary the Fig. from 13 to 16 can be utilized, but Fig. 13 (a) & (b) are utilized to illustrate the different interactive cases of PEV and Fig. 14 (a) & (b) and 15 (a) & (b) are utilized to demonstrate the charging and discharging condition of both PEVs. Fig. 16 (a) & (b) show the battery current characteristics curve of PI and ANFIS controller along with the current distortions. So, to demonstrate the research summary, here the Fig. 16 (a) & (b) are considered, and the summary is shown in a tabular form in Table 2.

VI. CONCLUSION

This study proposes an ANFIS controller to achieve coordinated power exchange between battery storage and the AC electrical grid through different mediators and controllers. A bi-directional power flow between the PEV and AC power grid is accomplished with the help of two ANFIS controllers and a proposed control strategy. The same scheme was carried out with PI controllers by replacing the two ANFIS controllers. Several technical issues were found in the second case while using PI controllers for the power management of PEVs' batteries. This was illustrated by the different characteristic curves of PEV's battery.

Two different ANFIS controllers were utilized to control the battery current and DC bus voltage, respectively, thus controlling the battery power. In the second case, because of using PI controller, there were very high starting surges and continuous distortion all over the active period of the battery and shown by different battery characteristics curves. The execution of the ANFIS controllers has overcome all these technical issues.

Another reason for choosing the ANFIS controller is that it utilizes an optimization technique, which saves time by making the system faster and contributing to sustainability.

Different simulation results have been performed to justify the contribution of the ANFIS controller over the PI controller. The proposed five operational modes of control strategy helped to manage the battery power management efficiency. Finally, both the proposed ANFIS controller and control algorithm provided a better power exchange and battery power management system.

In this study, no battery optimization technique was considered; using the optimization technique could provide better results in terms of battery power management. This will be done in a future research paper. Another limitation of this study is PEV's number, which can be improved by changing the control algorithm. Still, the lack of financial analysis of ANFIS controller over PI controller may create confusion among the consumers, and it can be considered as future work. Finally, the control algorithm used in this study shown in Fig. 9 is based on a relay control loop that can be carried out using a fuzzy controller. This could be another future development of this study.

TABLE 3. Battery characteristics, Li-ion (3.3V, 2.3 A h).

Listing	Standard
Voltage level	3.4 V
Resistance of internal	0.01 Ω
Polarization value	0.0076 Ω
The magnitude of the exponential area	0.26422 V
Reciprocal fixed time for exponential area	26.5487 $(Ah)^{-1}$
Weighing the value of cell	0.07 Kg
PEV bend slope	0.025
Energy value	7.59Wh

APPENDIX

See Table 3.

REFERENCES

[1] M. A. Hannan, M. S. H. Lipu, P. J. Ker, R. A. Begum, V. G. Agelidis, and F. Blaabjerg, "Power electronics contribution to renewable energy conversion addressing emission reduction: Applications, issues, and recommendations," *Appl. Energy*, vol. 251, Oct. 2019, Art. no. 113404.

[2] A. A. Z. Diab, H. M. Sultan, I. S. Mohamed, O. N. Kuznetsov, and T. D. Do, "Application of different optimization algorithms for optimal sizing of PV/wind/diesel/battery storage stand-alone hybrid microgrid," *IEEE Access*, vol. 7, pp. 119223–119245, 2019.

[3] S. Pazouki, A. Mohsenzadeh, and S. Member, "Simultaneous planning of PEV charging stations and DGs considering financial, technical, and environmental effects," *Can. J. Electr. Comput. Eng.*, vol. 38, no. 3, pp. 238–245, 2015.

[4] M. J. E. Alam, K. M. Muttaqi, and D. Sutanto, "Effective utilization of available PEV battery capacity for mitigation of solar PV impact and grid support with integrated V2G functionality," *IEEE Trans. Smart Grid*, vol. 7, no. 3, pp. 1562–1571, May 2016.

[5] A. Zakaria, F. B. Ismail, M. S. H. Lipu, and M. A. Hannan, "Uncertainty models for stochastic optimization in renewable energy applications," *Renew. Energy*, vol. 145, pp. 1543–1571, Jan. 2020.

[6] M. S. H. Lipu, M. S. Miah, M. A. Hannan, A. Hussain, M. R. Sarker, A. Ayob, M. H. M. Saad, and M. S. Mahmud, "Artificial intelligence based hybrid forecasting approaches for wind power generation: Progress, challenges and prospects," *IEEE Access*, vol. 9, pp. 102460–102489, 2021.

[7] H. Kraiem, A. Flah, N. Mohamed, M. Alowaidi, M. Bajaj, S. Mishra, N. K. Sharma, and S. K. Sharma, "Increasing electric vehicle autonomy using a photovoltaic system controlled by particle swarm optimization," *IEEE Access*, vol. 9, pp. 72040–72054, 2021.

[8] F. Aymen, M. Alowaidi, M. Bajaj, N. K. Sharma, S. Mishra, and S. K. Sharma, "Electric vehicle model based on multiple recharge system and a particular traction motor conception," *IEEE Access*, vol. 9, pp. 49308–49324, 2021.

[9] M. A. Hannan, D. N. T. How, M. S. H. Lipu, P. J. Ker, Z. Y. Dong, M. Mansur, and F. Blaabjerg, "SOC estimation of li-ion batteries with learning rate-optimized deep fully convolutional network," *IEEE Trans. Power Electron.*, vol. 36, no. 7, pp. 7349–7353, Jul. 2021.

[10] H. Liang, Y. Liu, F. Li, and Y. Shen, "Dynamic economic/emission dispatch including PEVs for peak shaving and valley filling," *IEEE Trans. Ind. Electron.*, vol. 66, no. 4, pp. 2880–2890, Apr. 2019.

[11] B. Viswanath, K. Revathi, and T. R. Jyothsna, "FACTS controllers for enhancement of power system performance: State-of-the-art," *Int. J. Pure Appl. Math.*, vol. 114, no. 8, pp. 265–273, 2017.

[12] M. S. H. Lipu, M. Faisal, S. Ansari, M. A. Hannan, T. F. Karim, A. Ayob, A. Hussain, M. Miah, and M. H. M. Saad, "Review of electric vehicle converter configurations, control schemes and optimizations: Challenges and suggestions," *Electronics*, vol. 10, no. 4, pp. 1–37, 2021.

[13] C. Aguilar-Ibanez, J. Moreno-Valenzuela, O. Garcia-Alarcon, M. Martinez-Lopez, J. A. Acosta, and M. S. Suarez-Castanon, "PI-type controllers and $\Sigma - \Delta$ modulation for saturated DC-DC buck power converters," *IEEE Access*, vol. 9, pp. 20346–20357, 2021.

[14] K. Benayad, T. Zabaiou, and A. Bouafassa, "Wide-area based SVC-fractional order PID controller for damping inter-area oscillations," in *Proc. 6th IEEE Int. Energy Conf. (ENERGYCon)*, Sep. 2020, pp. 610–615.

[15] H. Elwarfalli, A. Muntaser, J. Kumar, and G. Subramanyam, "Design and implementation of PI controller for the hybrid energy system," in *Proc. IEEE Nat. Aerosp. Electron. Conf. (NAECON) Ohio Innov. Summit (OIS)*, Jul. 2016, pp. 170–172.

[16] S. Khemakhem, M. Rekik, and L. Krichen, "A flexible control strategy of plug-in electric vehicles operating in seven modes for smoothing load power curves in smart grid," *Energy*, vol. 118, pp. 197–208, Jan. 2017.

[17] B. Gasbaoui, A. Nasri, and O. Abdelkhalek, "An efficiency PI speed controller for future electric vehicle in several topology," *Proc. Technol.*, vol. 22, pp. 501–508, Jan. 2016.

[18] S. V. K. Arun, U. Subramaniam, S. Padmanaban, M. S. Bhaskar, and D. Almakhles, "Investigation for performances comparison PI, adaptive PI, fuzzy speed control induction motor for centrifugal pumping application," in *Proc. IEEE 13th Int. Conf. Compat., Power Electron. Power Eng. (CPE-POWERENG)*, Apr. 2019, pp. 1–6.

[19] H. L. Lyu, W. Wang, X. P. Liu, and Z. Wang, "Modeling of multivariable fuzzy systems by semitensor product," *IEEE Trans. Fuzzy Syst.*, vol. 28, no. 2, pp. 228–235, Feb. 2020.

[20] G. Dyanamina and S. K. Kakodia, "Adaptive neuro fuzzy inference system based decoupled control for neutral point clamped multi level inverter fed induction motor drive," *Chin. J. Electr. Eng.*, vol. 7, no. 2, pp. 70–82, Jun. 2021.

[21] M. A. Hannan, Z. A. Ghani, M. M. Hoque, and M. S. H. Lipu, "A fuzzy-rule-based PV inverter controller to enhance the quality of solar power supply: Experimental test and validation," *Electronics*, vol. 8, no. 11, p. 1335, Nov. 2019.

[22] C. Osinski, G. V. Leandro, and G. H. da Costa Oliveira, "Fuzzy PID controller design for LFC in electric power systems," *IEEE Latin Amer. Trans.*, vol. 17, no. 1, pp. 147–154, Jan. 2019.

[23] H. H. Choi, H. M. Yun, and Y. Kim, "Implementation of evolutionary fuzzy PID speed controller for PM synchronous motor," *IEEE Trans. Ind. Informat.*, vol. 11, no. 2, pp. 540–547, Apr. 2015.

[24] F. Aymen, N. Mohamed, S. Chayma, C. H. R. Reddy, M. M. Alharthi, and S. S. M. Ghoneim, "An improved direct torque control topology of a double stator machine using the fuzzy logic controller," *IEEE Access*, vol. 9, pp. 126400–126413, 2021.

[25] C. S. Chin and W. P. Lin, "Robust genetic algorithm and fuzzy inference mechanism embedded in a sliding-mode controller for an uncertain underwater robot," *IEEE/ASME Trans. Mechatronics*, vol. 23, no. 2, pp. 655–666, Apr. 2018.

[26] N. K. Saxena and A. Kumar, "Voltage control using self trained ANFIS with probabilistic wind input and load pattern," in *Proc. Annu. IEEE India Conf. (INDICON)*, Dec. 2015, pp. 1–5.

[27] C. T. Krasopoulos, M. E. Beniakar, and A. G. Kladas, "Multicriteria PM motor design based on ANFIS evaluation of EV driving cycle efficiency," *IEEE Trans. Transport. Electrific.* , vol. 4, no. 2, pp. 525–535, Jun. 2018.

[28] N. Varghese and P. Reji, "Battery charge controller for hybrid stand alone system using adaptive neuro fuzzy inference system," in *Proc. Int. Conf. Energy Efficient Technol. Sustainability (ICEETS)*, Apr. 2016, pp. 171–175.

[29] E. H. M. Ndiaye, A. Ndiaye, M. Faye, and S. Gueye, "Intelligent control of a photovoltaic generator for charging and discharging battery using adaptive neuro-fuzzy inference system," *Int. J. Photoenergy*, vol. 2020, pp. 1–15, Mar. 2020.

[30] K. Kandasamy and R. Perumal, "Electric grid and vehicle integration using ANFIS controller in smart grid context," *Int. J. Adv. Comput. Electron. Eng.*, vol. 2, no. 4, pp. 14–19, 2017.

[31] K. Kandasamy, R. Perumal, and S. K. Velu, "ELM-ANFIS based controller for plug-in electric vehicle to grid integration," *Teh. Vjesn.*, vol. 25, no. 1, pp. 15–22, May 2018.

[32] M. A. Hannan, M. S. H. Lipu, A. Hussain, P. J. Ker, T. M. I. Mahlia, M. Mansor, A. Ayob, M. H. Saad, and Z. Y. Dong, "Toward enhanced state of charge estimation of lithium-ion batteries using optimized machine learning techniques," *Sci. Rep.*, vol. 10, no. 1, p. 4687, Dec. 2020.

[33] J. Han, X. Zhou, S. Lu, and P. Zhao, "A three-phase bidirectional grid-connected AC/DC converter for V2G applications," *J. Control Sci. Eng.*, vol. 2020, pp. 1–12, Sep. 2020.

[34] H. Wu, S.-C. Wong, C. K. Tse, and Q. Chen, "Control and modulation of bidirectional single-phase AC–DC three-phase-leg SPWM converters with active power decoupling and minimal storage capacitance," *IEEE Trans. Power Electron.*, vol. 31, no. 6, pp. 4226–4240, Jun. 2016.

[35] A. F. Ebrahim, A. A. S. Mohamed, A. A. Saad, and O. A. Mohammed, "Vector decoupling control design based on genetic algorithm for a residential microgrid system for future city houses at islanding operation," in *Proc. SoutheastCon*, Apr. 2018, pp. 1–5.

[36] N. Mohamed, F. Aymen, M. Alqarni, R. A. Turky, B. Alamri, Z. M. Ali, and S. H. E. A. Aleem, "A new wireless charging system for electric vehicles using two receiver coils," *Ain Shams Eng. J.*, pp. 1–15, Sep. 2021, doi: 10.1016/j.asej.2021.08.012.

[37] J. Meng, G. Luo, M. Ricco, M. Swierczynski, D.-I. Stroe, and R. Teodorescu, "Overview of lithium-ion battery modeling methods for state-of-charge estimation in electrical vehicles," *Appl. Sci.*, vol. 8, no. 5, p. 659, Apr. 2018.

[38] Z. Gao, C. Chin, W. Woo, and J. Jia, "Integrated equivalent circuit and thermal model for simulation of temperature-dependent $LiFePO_4$ battery in actual embedded application," *Energies*, vol. 10, no. 1, p. 85, Jan. 2017.

[39] E. Samadani, "Modeling of lithium-ion battery performance and thermal behavior in electrified vehicles," M.S. thesis, Dept. Mech. Eng., Univ. Waterloo, Waterloo, ON, Canada, 2015.

[40] A. Tessier, M. Dubois, and J. Trovão, "Real-time estimator li-ion cells internal resistance for electric vehicle application," *World Electr. Vehicle J.*, vol. 8, no. 2, pp. 410–421, Jun. 2016.

MD. ARIFUL ISLAM received the B.Sc. degree in electrical and electronic engineering (EEE) from the Ahsanullah University of Science and Technology (AUST), Dhaka, Bangladesh, in 2013, and the M.Eng. degree in electric power system management (EPSM) from the Asian Institute of Technology (AIT), Thailand, in 2019. Since 2015, he has been an Assistant Professor with the EEE Department, AUST. Prior to that, he also worked as an Assessor of electrical and fire safety at Sumerra, Bangladesh, which was an American project under alliance. His research interests include renewable energy technology and applications, power management, and load profile analysis on the distribution side. He was a recipient of the Asian Development Bank-Japanese Scholarship Program (ADB-JSP) to pursue his M.Eng. degree at AIT.

JAI GOVIND SINGH (Senior Member, IEEE) received the B.E. degree from MNNIT Allahabad, the M.Tech. degree from IIT Roorkee, and the Ph.D. degree from IIT Kanpur. Currently, he is working as an Associate Professor at the Department of Energy, Environment and Climate Change, SERD, Asian Institute of Technology (AIT), Bangkok, Thailand. Prior to joining AIT, he has worked as a Postdoctoral Research Associate at the KTH Royal Institute of Technology (KTH), Stockholm, Sweden, from 2008 to 2009, followed by The University of Queensland, Brisbane, Australia, as a Postdoctoral Research Fellow, in 2009. So far, he has supervised seven doctoral and 64 master's students, and has published more than 100 research papers in different peer-reviewed international journals and conference proceedings. His teaching and research interests include power systems planning, operation, and control; smart grid and microgrid; electric vehicles and battery storage; deregulation; solar and wind integration; and power distribution systems planning. He is a fellow of The Institution of Engineers, India.

ISRAT JAHAN was born in Cumilla, Bangladesh, in 1988. She received the B.Sc. degree in electrical and electronic engineering (EEE) from the Ahsanullah University of Science and Technology (AUST), Dhaka, Bangladesh, in 2011, where she is currently pursuing the M.Sc. degree in electric power system management (EPSM). Since 2013, she has been an Assistant Professor with the EEE Department, AUST. Her research interests include renewable energy technology and applications and PEV power management.

M. S. HOSSAIN LIPU received the B.Sc. degree in electrical and electronic engineering from the Islamic University of Technology, Bangladesh, in 2008, the M.Sc. degree in energy from the Asian Institute of Technology, Thailand, in 2013, and the Ph.D. degree in electrical, electronic, and systems engineering from Universiti Kebangsaan Malaysia (UKM), Malaysia, in 2019. He is currently a Senior Lecturer with the Department of Electrical, Electronic and Systems Engineering, UKM, where he is also the Coordinator at the Centre for Automotive Research (CAR). Prior to that, he worked as an Assistant Professor with the Department of Electrical and Electronic Engineering, University of Asia Pacific, Bangladesh. His research interests include battery storage and management systems, electric vehicles, power electronics, intelligent controllers, artificial intelligence, and optimization in renewable systems. He is the Guest Editor of *Sustainability* (MDPI).

TASKIN JAMAL (Senior Member, IEEE) received the bachelor's degree in electrical and electronic engineering from the Islamic University of Technology (IUT), Bangladesh (OIC Scholar), the master's degree in energy from the Asian Institute of Technology (AIT), Thailand (Japanese Govt. Scholar), and the Ph.D. degree in renewable energy from Murdoch University, Australia (IPRS and APA Scholar). He is currently serving as an Assistant Professor at the Ahsanullah University of Science and Technology (AUST), Bangladesh, and a Postdoctoral Research Associate at Keele University, U.K. He is also a part-time Lecturer at the Engineering Institute of Technology, Australia. Prior to joining AUST, he has taught in a number of universities across Australia, Bangladesh, Saudi Arabia, and Thailand. Throughout his academic career, he has earned a number of research and travel awards, the most recent of which was a research grant from the Climate Compatible Growth (CCG) Program, Foreign Development and Commonwealth Office (FCDO), U.K., for policy recommendations on Bangladesh's renewable energy deployment to the UN's Climate Change Conference, the COP26 summit in Glasgow, U.K., in 2021. His teaching and research interests include electric power systems planning, design, management and operation; microgrid; solar PV systems; renewable energy integration into grid; remote area electrification; and energy access. He is a member of IET. He serves as a Guest Editor for *Sustainability* (MDPI), *Energies* (MDPI), and *Sustainable Energy Technologies and Assessments* (Elsevier) journals and a Review Editor and a member of the Editorial Board for *Frontiers in Energy Research—Smart Grids*.

RAJVIKRAM MADURAI ELAVARASAN received the B.E. degree in electrical and electronics engineering from Anna University, Chennai, India, and the M.E. degree in power system engineering from the Thiagarajar College of Engineering, Madurai, India. He held an associate technical operations position with the IBM Global Technology Services Division. He was as an Assistant Professor with the Department of Electrical and Electronics, Sri Venkateswara College of Engineering, Sriperumbudur, Chennai. He was also a Visiting Scholar with the Clean and Resilient Energy Systems (CARES) Laboratory, Texas A&M University, Galveston, TX, USA. He is currently holding various positions in academia and industry, which are as follows: an Adjunct Faculty with the Department of Electrical and Electronics Engineering, Thiagarajar College of Engineering, and a Subject Matter Expert with the Research and Development Unit (Power and Energy), Nestlives Pvt. Ltd., Chennai. He has a Google citations of more than 1000. His research interests include renewable energy and smart grids, demand side management, multi criteria decision analysis, thermal energy storage, cyber-physical power systems, microgrids, power systems operation and control, and artificial intelligence-based control techniques. He was the department topper and a gold medalist in his master's degree. He has been a reviewer of more than 40 reputed SCIE journals.

LUCIAN MIHET-POPA (Senior Member, IEEE) was born in 1969. He received the bachelor's degree in electrical engineering, the master's degree in electric drives and power electronics, and the Ph.D. and Habilitation degrees in electrical engineering from the Politehnica University of Timisoara, Romania, in 1999, 2000, 2002, and 2015, respectively. Since 2016, he has been working as a Full Professor in energy technology with Østfold University College, Norway. From 1999 to 2016, he was with the Politehnica University of Timisoara. He has also worked as a Research Scientist with the Technical University of Denmark, from 2011 to 2014, and also with Aalborg University, Denmark, from 2000 to 2002. He held a postdoctoral position with the University of Siegen, Germany, in 2004. He is also the Head of the research laboratory "Intelligent Control of Energy Conversion and Storage Systems" and is one of the coordinators of the master's degree program in "green energy technology" with the Faculty of Engineering, Østfold University College. He has published more than 130 papers in national and international journals and conference proceedings, and ten books. He has participated in more than 15 international grants/projects, such as FP7, EEA, and Horizon 2020. He has been awarded more than ten national research grants. His research interests include modeling, simulation, control, and testing of energy conversion systems, and distributed energy resources (DER) components and systems, including battery storage systems (BSS) [for electric vehicles and hybrid cars and vanadium redox batteries (VRB)] and energy efficiency in smart buildings and smart grids. He has served as a Scientific and Technical Program Committee Member for many IEEE conferences. He was invited to join the energy and automotive committees by the President and the Honorary President of the Atomium European Institute, working in close cooperation with—under the umbrella—the EC and EU Parliament, and was also appointed as the Chairperson of AI4People, Energy Section. Since 2017, he has been a Guest Editor for five special issues of *Energies* (MDPI), *Applied Sciences*, *Majlesi Journal of Electrical Engineering*, and *Advances in Meteorology* journals.